

# Fermion-to-Fermion Low-Density Parity-Check Codes

Chong-Yuan Xu<sup>1,\*</sup>, Ze-Chuan Liu<sup>1,\*</sup> and Yong Xu<sup>1,2†</sup>

<sup>1</sup>Center for Quantum Information, IIIS, Tsinghua University, Beijing 100084, People's Republic of China and

<sup>2</sup>Hefei National Laboratory, Hefei 230088, PR China

Simulating fermionic systems on qubit-based quantum computers often demands significant computational resources due to the requirement to map fermions to qubits. Thus, designing a fault-tolerant quantum computer that operates directly with fermions offers an effective solution to this challenge. Here, we introduce a protocol for fault-tolerant fermionic quantum computation utilizing fermion-to-fermion low-density parity-check codes. Our method employs a fermionic low-density parity-check code memory, which transfers its state to fermionic color code processors assisted by lattice surgery, where logical operations are subsequently performed. To construct the fermionic low-density parity-check memory, we develop a systematic approach for creating fermionic stabilizer codes based on self-dual Calderbank-Shor-Steane codes. We present examples demonstrating these codes' significantly improved coding rate compared to the fermionic color code. Finally, we simulate the dynamics of a fermionic system using our protocol, illustrating effective error suppression.

The study of strongly correlated fermionic systems is central to high-energy physics [1], material science [2], and quantum chemistry [3], promising insights into phenomena ranging from quark dynamics [4] to high-temperature superconductivity [5]. However, solving these problems using classical computers is often very challenging. For instance, quantum Monte Carlo methods usually face the sign problem when addressing fermionic problems [6]. In this context, quantum computers offer a promising alternative [7]. However, since conventional quantum computers use qubits, solving fermionic problems requires mapping fermionic operators to qubit operators, which often incurs substantial overhead [8–13], making experimental implementation significantly challenging in the near term. To address this challenge, developing programmable fermionic quantum processors is increasingly appealing. In light of the unavoidable presence of noise, fault-tolerant fermionic quantum computing based on fermion-to-fermion repetition and color codes have been proposed very recently [14, 15]. However, the protocol's overhead remains substantial because the encoding rate is low, with each block encoding only a single logical fermion.

Recently, protocols based on quantum low-density parity-check (qLDPC) codes have been proposed to reduce the overhead in qubit-based fault-tolerant quantum computation [16–39]. Compared to the paradigmatic surface code, qLDPC codes feature a significantly higher coding rate. Although these codes require long-range connectivity between qubits, recent technological advances in platforms [37, 40–42] such as Rydberg atom arrays, superconducting qubits, and trapped ions have made the near-term implementation of these codes promising. Despite these significant advancements, existing studies primarily focus on constructing fault-tolerant quantum computers with qubits. It remains unclear how to construct a fermion-to-fermion LDPC code capable of encoding multiple fermion modes in a single code block and how to perform logical operations on such codes.

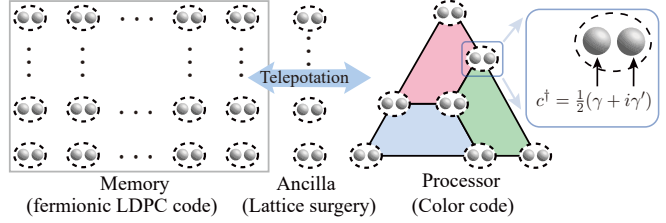


FIG. 1. Schematic illustration of fault-tolerant fermionic computation framework. The architecture comprises three components: fermionic memory implemented using fermionic LDPC codes, fermionic processor implemented using fermionic color codes to execute logical operations, and fermionic interface composed of ancilla fermions serving as a critical bridge for communication between memory and processor.

Here, we introduce a protocol for fault-tolerant fermionic quantum computation based on fermion-to-fermion LDPC codes. Our approach employs a fermionic LDPC memory integrated with fermionic color code processors as illustrated in Fig. 1, which is generalized from the qLDPC case. Logical fermionic information is initially stored in the fermionic LDPC memory and, when needed, is transferred to fermionic color code processors, where fault-tolerant logical operations are conducted. Upon completion, the information is returned to the memory. To construct the fermionic LDPC memory, we develop a systematic workflow for creating fermionic stabilizer codes based on self-dual Calderbank-Shor-Steane (CSS) codes. These codes are characterized by logical Majorana operators consisting of an odd number of physical Majorana operators. We construct three distinct classes of fermionic LDPC codes using three different LDPC codes: bicycle codes [43], finite Euclidean geometry codes [44, 45], and finite projective geometry codes [46]. These codes demonstrate a significantly improved coding rate compared to the fermionic color code. Furthermore, we propose a fault-tolerant method

to transfer logical fermionic states between the fermionic memory and processor via lattice surgery [47, 48]. We show that this process maintains the code distance. Finally, we simulate the dynamics of a fermionic system, demonstrating effective error suppression.

We start by introducing the construction of our fermionic LDPC codes from  $2n$  physical Majorana fermion operators  $\{\gamma_1, \gamma'_1, \gamma_2, \gamma'_2, \dots, \gamma_n, \gamma'_n\}$  arising from  $n$  physical complex fermion's creation and annihilation operators [49]. The strings of these Majorana operators, together with a phase factor  $\eta \in \{\pm 1, \pm i\}$ , generate the group of Majorana operators  $\text{Maj}(2n) \equiv \left\{ \Gamma = \eta \prod_{j=1}^n \gamma_j^{\alpha_j} (\gamma'_j)^{\alpha'_j} | \alpha_j, \alpha'_j \in \{0, 1\} \right\}$  [50]. The number of Majorana operators in  $\Gamma$  is referred to as its weight. The Majorana stabilizer code is defined by a Majorana stabilizer group  $\mathcal{S}_{\text{maj}}$ , a subgroup of  $\text{Maj}(2n)$ , where all elements are Hermitian, mutually commute, ensuring it is an Abelian subgroup, have even weight to preserve the parity of a physical fermion system, and  $-I$  with  $I$  being the identity element in the group is excluded [50]. The logical operators are generated by an independent subset of  $\text{Maj}(2n)$  comprising Majorana operator strings that commute with all elements of the stabilizer group  $\mathcal{S}_{\text{maj}}$  but are not members of  $\mathcal{S}_{\text{maj}}$  [51].

Each Majorana string operator can be represented by a binary vector  $(\alpha_1, \alpha'_1, \dots, \alpha_n, \alpha'_n)$ , where  $\alpha_j, \alpha'_j \in \{0, 1\}$  and  $1 \leq j \leq n$ . The binary vectors corresponding to the  $m$  independent stabilizer generators of  $\mathcal{S}_{\text{maj}}$  form an  $m \times n$  check matrix. For a fermion-to-fermion LDPC code, we construct a check matrix  $H$  based on a self-dual CSS code with the binary check matrices that satisfy  $H_X = H_Z = A$  and  $AA^T = 0$ , as follows,

$$H = \begin{pmatrix} H_\gamma & 0 \\ 0 & H_{\gamma'} \end{pmatrix}, \quad (1)$$

where  $H_\gamma = H_{\gamma'} = A$ .  $H_\gamma$  and  $H_{\gamma'}$  correspond to check matrices that characterize the stabilizers consisting exclusively of  $\{\gamma_j\}$  and  $\{\gamma'_j\}$  operators, respectively, as described for fermion-to-fermion color codes in Ref. [14]. The logical operators are represented by vectors in the kernel of  $H$  that cannot be generated by stabilizers, forming a homology group  $\ker(A)/\text{im}(A)$  for both  $\gamma$  and  $\gamma'$  types of logical operators [52].

In our protocol, there are multiple logical fermions within a single fermionic LDPC memory, and these logical fermions are transferred to processors for the execution of logical operations. It is essential that the logical Majorana operator in memory anticommutes with that in the processor to adhere to fermionic statistics. We thus require all logical Majorana operators in memory have odd weight and even overlap with each other [50]. Such conditions also ensure that the fermionic statistics are maintained when concatenating different fermionic code blocks [14]. We denote the logical Majorana operators as  $\bar{\gamma}_j$  and  $\bar{\gamma}'_j$  with  $1 \leq j \leq k$  ( $k$  is the number of

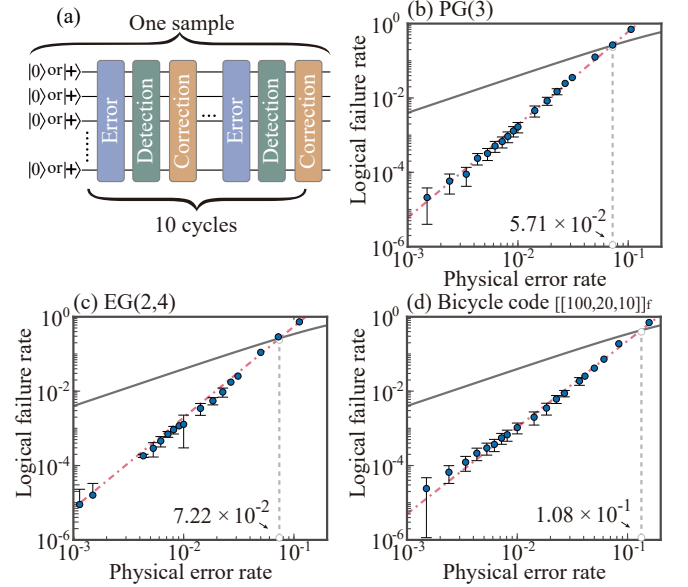


FIG. 2. (a) Error model used to benchmark the capacity of our fermionic LDPC code memory. Each sample consists of 10 cycles, each incorporating three layers: random errors, syndrome measurements, and error correction. (b)-(d) The numerically calculated logical failure rate with respect to the physical error rate for three fermionic LDPC codes: PG(2,3), EG(2,3), and Bicycle code [[100,20,10]]<sub>f</sub>. The dashed red line indicates a power law fit to the data, and the gray line represents the case where the logical and physical error rates are equal. The vertical dashed gray line highlights the code's pseudo-threshold.

logical complex fermions), which consist of physical Majorana operators  $\{\gamma_1, \dots, \gamma_n\}$  and  $\{\gamma'_1, \dots, \gamma'_n\}$ , respectively. The logical complex fermion creation operators are then defined as  $\bar{c}_j^\dagger = \frac{1}{2}(\bar{\gamma}_j + i\bar{\gamma}'_j)$  [49].

Previous studies have primarily focused on encoding Majorana modes into qubits, lacking methods for identifying odd-weight logical operators within codes [50, 53, 54]. To identify them, we generalize the Gram-Schmidt orthogonalization process to vector spaces over  $\mathbb{F}_2$  [55]. Let  $\{\vec{\gamma}_j | j = 1, \dots, k', k' \geq k\}$  be a basis for  $\ker A/\text{im}(A)$ , which is itself also a vector space;  $\vec{\gamma}_j$  represents the corresponding logical  $\bar{\gamma}_j$  or  $\bar{\gamma}'_j$  operator, expressed as  $\gamma_1^{[\vec{\gamma}_j]_1} \dots \gamma_n^{[\vec{\gamma}_j]_n}$  or  $(\gamma'_1)^{[\vec{\gamma}_j]_1} \dots (\gamma'_n)^{[\vec{\gamma}_j]_n}$ . If there exists a basis vector with odd number of 1's, say  $\vec{\gamma}_1$ , we remove it from the basis and make the remaining basis vectors orthogonal to it via  $\vec{\gamma}_j \rightarrow \vec{\gamma}_j - (\vec{\gamma}_1 \cdot \vec{\gamma}_j)\vec{\gamma}_1$ , i.e.,  $\vec{\gamma}_1$  has even overlap with all others. This procedure is repeated until no odd-weight basis vector remains. The obtained odd-weight vectors correspond to logical operators which have odd weight, and the overlap weight between any two of them is even, thus satisfying the fermionic anticommutation relation. The necessary and sufficient condition for the existence of at least one odd-weight logical is  $(1, 1, \dots, 1)^T \notin \text{im}(A)$  (see Supplemental Material). We also prove that the procedure always produces a maxi-

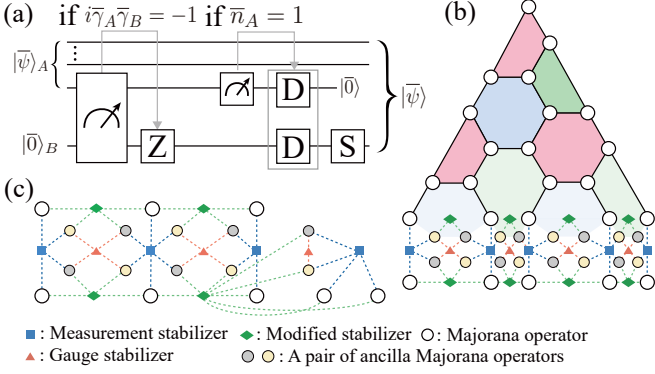


FIG. 3. (a) Quantum circuit to transfer a logical fermionic state  $|\bar{\psi}\rangle_A$  to code block  $B$  (initialized as  $|\bar{0}\rangle_B$ ). The protocol involves: (i) measuring  $i\bar{\gamma}_A\bar{\gamma}_B$  and applying the  $Z$  gate of  $\exp(i\pi\bar{n}_A)$ , provided the measurement result is  $-1$ ; (ii) measuring the logical particle number  $\bar{n}_A$  and applying the  $D$  gate defined as  $\bar{D} = \exp(i\pi\bar{\gamma})$  to both code block  $A$  and  $B$  if the measurement outcome is  $1$ . The validation of this circuit is provided in Supplemental material. (b) Illustration of the lattice surgery for fault-tolerant measurements of  $i\bar{\gamma}_A\bar{\gamma}_B$  for a case with  $|\bar{\gamma}_A| = |\bar{\gamma}_B|$ . In this example, code  $B$  is a  $d = 5$  fermionic color code, and code  $A$  is a fermionic LDPC code containing five Majorana operators in the support of  $\bar{\gamma}_A$ . The empty circles represent the  $\gamma$ -type Majorana operators in blocks  $A$  and  $B$ . Several pairs of ancilla Majorana operators are introduced with each horizontal pair represented by yellow and gray circles to denote  $\gamma$ -type and  $\gamma'$ -type Majorana operator forming a complex fermion. The  $\gamma$ -type stabilizer generators at the boundary, connected to ancilla fermions, are modified to incorporate the ancilla Majorana operators (green rhombuses). Measurement and gauge stabilizer generators are depicted as blue squares and red triangles, respectively. The product of these stabilizer generators yields the joint logical operator  $i\bar{\gamma}_A\bar{\gamma}_B$ . The  $\gamma'$ -type Majorana stabilizers remain unchanged. The general procedure for introducing ancilla Majorana operators and constructing the corresponding stabilizers is detailed in Supplemental Material. (d) A more general fermionic lattice surgery scheme for two fermionic LDPC codes with arbitrary weights.

mumally linearly independent set of odd-weight binary vectors (see Supplemental Material). In this case, the resulting odd-weight logical operators define a fermionic subspace code for our fermionic LDPC code. In addition, we provide a necessary and sufficient condition under which all basis vectors can be used to generate odd-weight logical operators in Supplemental Material.

Based on three different LDPC codes, which include finite projective geometry codes [46], finite Euclidean geometry codes [44, 45], and bicycle codes [43], we construct three classes of fermionic LDPC codes (see Supplemental Material for detailed construction methods). We find that these subspace fermionic LDPC codes yield the same or nearly the same encoding rate as the original ones. We consider one code from each type and benchmark their logical information resilience as a fermion memory through numerical simulations. Specifically, we initial-

ize the logical state in  $|\bar{0}\bar{0}\dots\bar{0}\rangle$ , a logical fermionic vacuum state without any logical fermions, and simulate errors occurring as physical single-fermion gate  $\gamma_j$ ,  $\gamma'_j$ , and  $i\gamma_j\gamma'_j$  with equal probability  $p/3$ , where  $p$  denotes the physical error rate. Subsequently, we perform error detection via syndrome measurements (assuming perfect syndrome measurements for simplicity), followed by error decoding using the belief propagation and ordered-statistical decoding (BP+OSD) algorithm [56, 57]. After decoding, we correct errors by applying physical single-fermion gates and then repeat the entire process for the corrected new state. For each sample, we conduct  $N_c = 10$  rounds of error-correction circuit cycles (each cycle contains three layers: random errors, syndrome measurements, and error correction), as shown in Fig. 2(a). The logical error probability for each sample is defined as  $P_L(N_c) = N_{\text{error}}/N_{\text{sample}}$ , where  $N_{\text{error}}$  and  $N_{\text{sample}}$  denote the number of erroneous trials and total trials, respectively. The logical failure rate is then  $p_L = 1 - (1 - P_L(N_c))^{1/N_c}$  [36, 37]. Figure 2 shows the logical error rate with respect to the physical error rate for the finite projective geometry PG(3) code, the finite Euclidean geometry EG(2, 4) code, and the  $[[100, 20, 10]]_F$  bicycle code. We clearly see that the logical error rate is significantly suppressed compared to the physical one according to  $p_L \sim p^\alpha$  with  $\alpha \approx 2$ . Following the convention [37], we define the code's pseudo-threshold as the solution to the break-even equation  $p_L(p) = P(p, k)$ , where  $P(p, k)$  is the probability of at least one error occurring on  $k$  physical fermion sites at physical error rate  $p$ . Under this error model, all three codes exhibit relatively high pseudo-thresholds.

In Supplemental Material, we also study several other self-dual codes such as Kitaev Majorana code [49] and unicycle codes [43]. We find that they are not suitable for producing well-behaved fermionic LDPC because they do not support the generation of odd-weight logical operators.

We now study how to perform logical operations on the fermionic LDPC memory. Instead of executing logical gates directly on the fermionic LDPC, we consider a method whereby the states of a target logical fermion mode in memory are transferred to an external fermionic color code processor. Logical operations are then performed on these processors, and the states are subsequently transferred back to the memory. This approach is inspired by fault-tolerant measurements of logical operators in qubit LDPC codes [30, 36, 58]. If the logical operation involves two logical fermion modes, we consider two color code processors. The logical information of the two fermion modes is individually transferred, logical operations are applied between these two color code blocks, and the information is subsequently returned to memory. Logical operations involving more logical fermion modes can be performed similarly. For fermionic state transfers between memory and processor,

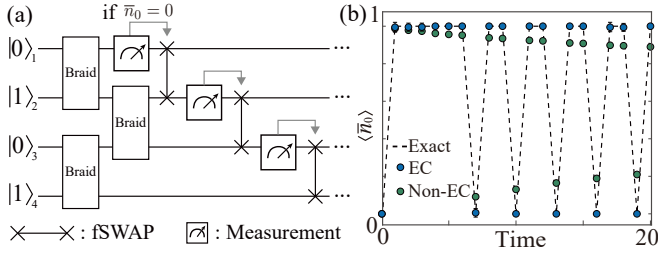


FIG. 4. (a) The quantum circuit used to benchmark our scheme. We first initialize the system in the logical state  $|0101\rangle$  and then apply three braid gates with each gate executing the operation  $B_{j,j+1} = \exp(i\pi(\bar{c}_j^\dagger \bar{c}_{j+1} + \text{H.c.})/2)$ . On-site measurements of  $\bar{n}_j = \bar{c}_j^\dagger \bar{c}_j$  with  $j = 0, 1, 2$  are then performed, followed by a fermionic swap (fSWAP) gate if the measurement result is zero. The unitary gates and feedback process constitute a module, which is executed consecutively multiple times. (b) The expectation value of  $\bar{n}_0$  with respect to time which is characterized by the number of executed modules. We see that the simulation under noise with error correction (filled blue circles) is very close to the noiseless simulation result (black dashed line), in stark contrast to the simulation results under noise without error correction (filled green circles).

we design a measurement-based circuit as illustrated in Fig. 3(a). This circuit enables the transfer of a single logical fermion information described by logical Majorana operators  $\bar{\gamma}_A$  and  $\bar{\gamma}'_A$  to a processor described by logical Majorana operators  $\bar{\gamma}_B$  and  $\bar{\gamma}'_B$ , which is initialized in the logical vacuum state  $|\bar{0}\rangle_B$ . In other words, an output state is the same as the initial state except that the processor logical fermion plays the role of the corresponding logical fermion in memory. During the transfer, a key step is the fault-tolerant measurement of the joint logical operator  $i\bar{\gamma}_A \bar{\gamma}_B$ , as shown in Fig. 3(a).

We propose fermionic lattice surgery to realize the fault-tolerant joint measurement as shown in Fig. 3(b) and (c). Let  $d_A$  be the weight of  $\bar{\gamma}_A$  and  $\bar{\gamma}'_A$ . For simplicity, we consider the case where block  $B$  is a color code whose distance satisfies that  $d_B = d_A$  and put the general case where block  $B$  is also a fermionic LDPC code in Supplemental Material. To realize the measurement, we align the support of the logical operator  $\bar{\gamma}_A$  and  $\bar{\gamma}_B$  and introduce a set  $Q_C$  of  $4(d_A - 1)$  ancilla Majorana operators (corresponding to  $2(d_A - 1)$  complex fermions) between these two codes, labeled as  $\gamma_{a,1}, \gamma'_{a,1}, \dots, \gamma_{a,(d_A-1)}, \gamma'_{a,(d_A-1)}$  and  $\gamma_{b,1}, \gamma'_{b,1}, \dots, \gamma_{b,(d_A-1)}, \gamma'_{b,(d_A-1)}$ . The original  $\gamma$ -type stabilizer generators at the boundary are modified by including two ancilla Majorana operators as shown in Fig. 3(b). Measurement stabilizer generators  $M_1, M_2, \dots, M_{d_A}$  and gauge stabilizer generators  $G_1, G_2, \dots, G_{d_A-1}$  are also introduced. The original  $\gamma'$ -type stabilizer generators for both block of  $A$  and  $B$  are not modified. This merging procedure creates a merged stabilizer code  $\mathcal{C}_{\text{merged}}$  where

$i\bar{\gamma}_A \bar{\gamma}_B$  becomes a stabilizer. Since  $2(d_A - 1)$  ancilla complex fermions and  $2d_A - 1$  new stabilizers are introduced, this new code only contains one logical complex fermion described by  $\bar{\gamma}'_A$  and  $\bar{\gamma}'_B$ . In other words, one cannot find  $\gamma$ -type logical operators in the merged code. In this case, we show that the merging procedure does not decrease the code distance based on the formalism of the subsystem code (see Supplemental Material). The number of the Majorana modes introduced during the whole process is small compared to the fermionic LDPC memory, resulting in a small resource overhead (see Supplemental Material). The Supplemental Material also provides the general guidelines for introducing ancilla Majorana operators and constructing stabilizer generators. Moreover, we propose a more comprehensive scheme for performing lattice surgery between two fermionic stabilizer codes (see Fig. 3(c) for an example) with details in Supplemental Material.

To achieve the fault-tolerant measurement of  $i\bar{\gamma}_A \bar{\gamma}_B$ , we first initialize the physical ancilla complex fermions in the  $|0\rangle$  state and then measure all the stabilizer generators in the merged code and perform  $\min\{d_A, d_B\}$  round of error corrections in the presence of noisy measurements to ensure fault-tolerance. Finally, each physical ancilla fermion is measured in the particle number basis to return the state to the original code space.

We now demonstrate the capability of our codes by simulating the quantum circuit of fermions shown in Fig. 4(a). The circuit incorporates braid operations that enable the tunneling of fermions between neighboring sites, and onsite measurements, followed by fermionic swap gates, provided the measurement outcome is zero. For an initial state  $|0101\rangle$ , we expect that the steady state of this dynamical process is characterized by the particle occupation number at the upper boundary exceeding the average particle occupation number of  $1/2$  due to feedback effects [59–61]. To simulate the dynamic behavior, we utilize the PG(3) code as our fermionic LDPC code and select four encoded complex fermion modes from it. Additionally, we introduce two copies of the fermionic Steane code to function as processors. The calculated time evolution of the particle number at the first site, denoted  $\langle \hat{n}_0 \rangle$ , is shown in Fig. 4(b). The value of  $\langle \hat{n}_0 \rangle$  exhibits oscillatory behavior, but the time-averaged value is larger than  $1/2$ , which aligns with the expected characteristics of a skin state. Notably, with our fault-tolerant logical operations and error correction techniques, the error-corrected data demonstrate significantly higher fidelity compared to the uncorrected data, as shown in Fig. 4(b). The time evolution results using the general lattice surgery is provided in Supplemental Material.

In summary, we have developed a systematic workflow for constructing fermionic LDPC code memory based on self-dual CSS codes and proposed methods for executing logical operations based on lattice surgery. We demonstrate that our fermionic LDPC code can be used to sim-

ulate dynamics of fermionic systems fault-tolerantly with effective error detection and correction. Such fermion-to-fermion quantum computation has the potential to significantly reduce the computational complexity associated with simulating fermionic systems, leveraging the possibility of achieving quantum advantage in quantum simulations. Our work encourages the pursuit of high-performance fermionic LDPC codes with higher code rates and larger code distances, as well as the advancement of more efficient methods for executing logical operations with reduced overhead.

*Note added.* During the final stage of this work, we became aware of a related work [62], which uses Majorana LDPC codes to encode logical qubits. In contrast, we encode logical fermions with Majorana LDPC codes, and our fermionic state transfer protocol provides an alternative method to perform logical operations with low overhead.

We thank Y. Li, Q. Xu, and F. Wei for helpful discussions. This work is supported by the National Natural Science Foundation of China (Grant No. 12474265 and No. 11974201) and Innovation Program for Quantum Science and Technology (Grant No. 2021ZD0301604). We also acknowledge the support by center of high performance computing, Tsinghua University.

Rev. A **64**, 022319 (2001).

- [10] S. B. Bravyi and A. Y. Kitaev, Fermionic quantum computation, Ann. Phys. **298**, 210 (2002).
- [11] R. C. Ball, Fermions without fermion fields, Phys. Rev. Lett. **95**, 176407 (2005).
- [12] F. Verstraete and J. I. Cirac, Mapping local hamiltonians of fermions to local hamiltonians of spins, J. Stat. Mech.: Theory Exp. **2005** (09), P09012.
- [13] J. D. Whittfield, V. c. v. Havlíček, and M. Troyer, Local spin operators for fermion simulations, Phys. Rev. A **94**, 030301 (2016).
- [14] A. Schuckert, E. Crane, A. V. Gorshkov, M. Hafezi, and M. J. Gullans, Fermion-qubit fault-tolerant quantum computing, arXiv:2411.08955 (2024).
- [15] R. Ott, D. González-Cuadra, T. V. Zache, P. Zoller, A. M. Kaufman, and H. Pichler, Error-corrected fermionic quantum processors with neutral atoms, arXiv:2412.16081 (2024).
- [16] J.-P. Tillich and G. Zémor, Quantum ldpc codes with positive rate and minimum distance proportional to the square root of the blocklength, IEEE Transactions on Information Theory **60**, 1193 (2013).
- [17] D. Gottesman, Fault-tolerant quantum computation with constant overhead, Quantum Information and Computation **14**, 1338 (2013).
- [18] A. A. Kovalev and L. P. Pryadko, Quantum kronecker sum-product low-density parity-check codes with finite rate, Phys. Rev. A **88**, 012311 (2013).
- [19] N. P. Breuckmann and B. M. Terhal, Constructions and noise threshold of hyperbolic surface codes, IEEE transactions on Information Theory **62**, 3731 (2016).
- [20] P. Panteleev and G. Kalachev, Degenerate quantum ldpc codes with good finite length performance, Quantum **5**, 585 (2021).
- [21] N. P. Breuckmann and J. N. Eberhardt, Balanced product quantum codes, IEEE Transactions on Information Theory **67**, 6653 (2021).
- [22] A. Krishna and D. Poulin, Fault-tolerant gates on hypergraph product codes, Phys. Rev. X **11**, 011023 (2021).
- [23] O. Higgott and N. P. Breuckmann, Subsystem codes with high thresholds by gauge fixing and reduced qubit overhead, Phys. Rev. X **11**, 031039 (2021).
- [24] N. P. Breuckmann and J. N. Eberhardt, Quantum low-density parity-check codes, PRX quantum **2**, 040101 (2021).
- [25] P. Panteleev and G. Kalachev, Quantum ldpc codes with almost linear minimum distance, IEEE Transactions on Information Theory **68**, 213 (2021).
- [26] N. Delfosse, M. E. Beverland, and M. A. Tremblay, Bounds on stabilizer measurement circuits and obstructions to local implementations of quantum ldpc codes, arXiv:2109.14599 (2021).
- [27] N. Baspin and A. Krishna, Connectivity constrains quantum codes, Quantum **6**, 711 (2022).
- [28] N. Baspin and A. Krishna, Quantifying nonlocality: How outperforming local quantum codes is expensive, Phys. Rev. Lett. **129**, 050505 (2022).
- [29] M. A. Tremblay, N. Delfosse, and M. E. Beverland, Constant-overhead quantum error correction with thin planar connectivity, Phys. Rev. Lett. **129**, 050504 (2022).
- [30] L. Z. Cohen, I. H. Kim, S. D. Bartlett, and B. J. Brown, Low-overhead fault-tolerant quantum computing using long-range connectivity, Sci. Adv. **8**, eabn1717 (2022).
- [31] P. Panteleev and G. Kalachev, Asymptotically good

\* These authors contribute equally to this work.

† [yongxuphy@tsinghua.edu.cn](mailto:yongxuphy@tsinghua.edu.cn)

- [1] C. W. Bauer, Z. Davoudi, A. B. Balantekin, T. Bhattacharya, M. Carena, W. A. De Jong, P. Draper, A. El-Khadra, N. Gemelke, M. Hanada, *et al.*, Quantum simulation for high-energy physics, PRX quantum **4**, 027001 (2023).
- [2] B. Bauer, S. Bravyi, M. Motta, and G. K.-L. Chan, Quantum algorithms for quantum chemistry and quantum materials science, Chem. Rev. **120**, 12685 (2020).
- [3] S. McArdle, S. Endo, A. Aspuru-Guzik, S. C. Benjamin, and X. Yuan, Quantum computational chemistry, Rev. Mod. Phys. **92**, 015003 (2020).
- [4] J. Berges, M. P. Heller, A. Mazeliauskas, and R. Venugopalan, Qcd thermalization: Ab initio approaches and interdisciplinary connections, Rev. Mod. Phys. **93**, 035003 (2021).
- [5] C. M. Varma, Colloquium: Linear in temperature resistivity and associated mysteries including high temperature superconductivity, Rev. Mod. Phys. **92**, 031001 (2020).
- [6] M. Troyer and U.-J. Wiese, Computational complexity and fundamental limitations to fermionic quantum monte carlo simulations, Phys. Rev. Lett. **94**, 170201 (2005).
- [7] R. P. Feynman, Simulating physics with computers, Int. J. Theor. Phys. **21**, 467 (1982).
- [8] D. S. Abrams and S. Lloyd, Simulation of many-body fermi systems on a universal quantum computer, Phys. Rev. Lett. **79**, 2586 (1997).
- [9] G. Ortiz, J. E. Gubernatis, E. Knill, and R. Laflamme, Quantum algorithms for fermionic simulations, Phys.

quantum and locally testable classical ldpc codes, in *Proceedings of the 54th annual ACM SIGACT symposium on theory of computing* (2022) pp. 375–388.

[32] A. Leverrier and G. Zémor, Quantum tanner codes, in *2022 IEEE 63rd Annual Symposium on Foundations of Computer Science (FOCS)* (IEEE, 2022) pp. 872–883.

[33] A. Strikis and L. Berent, Quantum low-density parity-check codes for modular architectures, *PRX Quantum* **4**, 020321 (2023).

[34] A. O. Quintavalle, P. Webster, and M. Vasmer, Partitioning qubits in hypergraph product codes to implement logical gates, *Quantum* **7**, 1153 (2023).

[35] H.-K. Lin and L. P. Pryadko, Quantum two-block group algebra codes, *Phys. Rev. A* **109**, 022407 (2024).

[36] Q. Xu, J. P. Bonilla Ataides, C. A. Pattison, N. Raveendran, D. Bluvstein, J. Wurtz, B. Vasić, M. D. Lukin, L. Jiang, and H. Zhou, Constant-overhead fault-tolerant quantum computation with reconfigurable atom arrays, *Nat. Phys.* **20**, 1084 (2024).

[37] S. Bravyi, A. W. Cross, J. M. Gambetta, D. Maslov, P. Rall, and T. J. Yoder, High-threshold and low-overhead fault-tolerant quantum memory, *Nature* **627**, 778 (2024).

[38] G. Zhang and Y. Li, Time-efficient logical operations on quantum low-density parity check codes, *Phys. Rev. Lett.* **134**, 070602 (2025).

[39] Y. Li, Low-density parity-check representation of fault-tolerant quantum circuits, *Phys. Rev. Res.* **7**, 013115 (2025).

[40] D. Bluvstein, H. Levine, G. Semeghini, T. T. Wang, S. Ebadi, M. Kalinowski, A. Keesling, N. Maskara, H. Pichler, M. Greiner, *et al.*, A quantum processor based on coherent transport of entangled atom arrays, *Nature* **604**, 451 (2022).

[41] D. Bluvstein, S. J. Evered, A. A. Geim, S. H. Li, H. Zhou, T. Manovitz, S. Ebadi, M. Cain, M. Kalinowski, D. Hangleiter, *et al.*, Logical quantum processor based on reconfigurable atom arrays, *Nature* **626**, 58 (2024).

[42] J.-S. Chen, E. Nielsen, M. Ebert, V. Inlek, K. Wright, V. Chaplin, A. Maksymov, E. Páez, A. Poudel, P. Maunz, *et al.*, Benchmarking a trapped-ion quantum computer with 30 qubits, *Quantum* **8**, 1516 (2024).

[43] D. J. C. MacKay, G. Mitchison, and P. L. McFadden, Sparse-graph codes for quantum error correction, *IEEE Transactions on Information Theory* **50**, 2315 (2004).

[44] D. Cao, Y. Song, and S. Zhao, A novel construction of quantum ldpc codes based on cyclic classes of lines in euclidean geometries, *Journal of electronics (China)* **29**, 1 (2012).

[45] S. A. Aly, A class of quantum ldpc codes constructed from finite geometries, in *IEEE GLOBECOM 2008-2008 IEEE Global Telecommunications Conference* (IEEE, 2008) pp. 1–5.

[46] J. Farinholt, Quantum ldpc codes constructed from point-line subsets of the finite projective plane, *arXiv:1207.0732* (2012).

[47] D. Horsman, A. G. Fowler, S. Devitt, and R. Van Meter, Surface code quantum computing by lattice surgery, *New J. Phys.* **14**, 123011 (2012).

[48] A. G. Fowler and C. Gidney, Low overhead quantum computation using lattice surgery, *arXiv:1808.06709* (2018).

[49] A. Kitaev, Anyons in an exactly solved model and beyond, *Ann. Phys.* **321**, 2 (2006).

[50] S. Bravyi, B. M. Terhal, and B. Leemhuis, Majorana fermion codes, *New J. Phys.* **12**, 083039 (2010).

[51] M. A. Nielsen and I. L. Chuang, *Quantum computation and quantum information* (Cambridge university press, 2010).

[52] H. Bombin and M. A. Martin-Delgado, Homological error correction: Classical and quantum codes, *J. Math. Phys.* **48**, 052105 (2007).

[53] D. Litinski and F. von Oppen, Quantum computing with majorana fermion codes, *Phys. Rev. B* **97**, 205404 (2018).

[54] S. Vijay, T. H. Hsieh, and L. Fu, Majorana fermion surface code for universal quantum computation, *Phys. Rev. X* **5**, 041038 (2015).

[55] Y. Prasetia, R. Kurnia, A. Andriko, and P. Astuti, Extended gram-schmidt process on sesquilinear spaces over finite fields, *International Electronic Journal of Algebra* **1** (2025).

[56] J. Liang, Q. Wang, L. Li, L. Song, and X. Ma, A low-complexity bp-osd algorithm for quantum ldpc codes, *The European Physical Journal Special Topics* **1** (2025).

[57] Decoding across the quantum low-density parity-check code landscape, **2**.

[58] H. Poulsen Nautrup, N. Friis, and H. J. Briegel, Fault-tolerant interface between quantum memories and quantum processors, *Nat. Commun.* **8**, 1321 (2017).

[59] Y.-P. Wang, C. Fang, and J. Ren, Absence of measurement-induced entanglement transition due to feedback-induced skin effect, *Phys. Rev. B* **110**, 035113 (2024).

[60] X. Feng, S. Liu, S. Chen, and W. Guo, Absence of logarithmic and algebraic scaling entanglement phases due to the skin effect, *Phys. Rev. B* **107**, 094309 (2023).

[61] Z.-C. Liu, K. Li, and Y. Xu, Dynamical transition due to feedback-induced skin effect, *Phys. Rev. Lett.* **133**, 090401 (2024).

[62] M. Mudassar, A. Schuckert, and D. Gottesman, Fault tolerant operations in majorana-based quantum codes: Gates, measurements and high rate constructions, *arXiv:2508.09928* (2025).